Accepted Manuscript

Silica nanospheres entrapped with ultra-small luminescent crystals for protein delivery

Yangyang Li, Xiaoyi Chen, Heng Liu, Xiaozhou Mou, Zhaohui Ren, Zeeshan Ahmad, Xiang Li, Gaorong Han

PII: S1385-8947(17)31220-2
DOI: http://dx.doi.org/10.1016/j.cej.2017.07.073
Reference: CEJ 17339

To appear in: *Chemical Engineering Journal*

Received Date: 17 January 2017
Revised Date: 10 July 2017
Accepted Date: 12 July 2017

Please cite this article as: Y. Li, X. Chen, H. Liu, X. Mou, Z. Ren, Z. Ahmad, X. Li, G. Han, Silica nanospheres entrapped with ultra-small luminescent crystals for protein delivery, *Chemical Engineering Journal* (2017), doi: http://dx.doi.org/10.1016/j.cej.2017.07.073

This is a PDF file of an unedited manuscript that has been accepted for publication. As a service to our customers we are providing this early version of the manuscript. The manuscript will undergo copyediting, typesetting, and review of the resulting proof before it is published in its final form. Please note that during the production process errors may be discovered which could affect the content, and all legal disclaimers that apply to the journal pertain.

ACCEPTED MANUSCRIPT

Silica nanospheres entrapped with ultra-small luminescent crystals for protein delivery

Yangyang Li [a], Xiaoyi Chen [b], Heng Liu [a], Xiaozhou Mou [b], Zhaohui Ren [a], Zeeshan Ahmad [c], Xiang Li *[a], Gaorong Han[a]

[a] *State Key Laboratory of Silicon Materials, School of Materials Science and Engineering, Zhejiang University, Hangzhou, P.R. China 310027*
[b] *Clinical Research Institute, Zhejiang Provincial People's Hospital, Hangzhou, 310014, P. R. China*
[c] *School of Pharmacy, De Montfort University, Leicester LE1 9BH, UK*

*Corresponding Author: xiang.li@zju.edu.cn (X. Li)

Abstract

Constructing smart nano-systems for intracellular delivery of functional proteins has been endeavored for diverse biomedical applications, but suffered daunting challenges. Herein silica nanospheres entrapped with photoluminescent CaF_2:Tm,Yb nanocrystals were synthesized and decorated with amino molecules for protein delivery. Amino-modified nanospheres presented high protein loading capacity and sustained release phenomenon. The photoluminescence of particles highly corresponded to protein release progress. The preliminary *in-vitro* study confirmed markedly enhanced cell up-taking efficiency of protein molecules with the nanocomposite developed.

Keywords: Intracellular protein delivery; photoluminescence; silica nanospheres.

ACCEPTED MANUSCRIPT

1. Introduction

Intracellular delivery with certain proteins plays a fundamental role in diverse biomedical applications, from restoring the function of interest, producing highly specific molecules in situ, to regulating gene expression without minimal genomic alteration [1,2]. The main mechanism is to deliver protein complex (e.g., multicomponent protein assemblies or post-translationally modified proteins) into cells in a rational manner as these proteins require exquisite cellular machinery for production, which may not be present or fully functional in the host cell [3,4]. However, in general physiological environment, most of proteins intend to undergo degradation by proteolytic enzymes or, in the case of the higher-molecular-weight proteins, may be recognized by neutralizing antibodies [5,6]. The fragility of most therapeutic proteins and impermeability of cell membrane limit effective intracellular delivery of protein molecules [7]. In general, two criteria for enabling expected protein therapy shall be met: transportation to cell cytoplasm and retention of biological activity at the targeted site of action [8]. An efficient protocol for intracellular delivery of native, functional proteins, in an active conformation, is of crucial significance, but suffered daunting challenges.

In the past decade, nanocarrier-based approaches, such as mesoporous silica nanoparticles (MSNs), for intracellular protein delivery have attracted considerable interest worldwide [9, 10]. Slowing *et al.* reported successful intracellular delivery of membrane-impermeable protein cytochrome c (Cyto C) using MSNs [11]. Bale *et al.* demonstrated that silica nanoparticles enabled effective intracellular delivery of Ribonuclease A (RNase A) [4]. Conventional silica nanoparticles, where only external surface can be utilized for protein attachment due to the large dimensions of macromolecules [12], may induce low protein loading capacity and burst release. Meanwhile, silica hollow spheres, synthesized with current hard templating and microemulsion approaches, may present large pores (>10 nm) [13], but its particle size in the micrometer range hinders the up-taking behavior of cells. Therefore, the investigation of silica nanospheres endowed with low dimensions as well as new

ACCEPTED MANUSCRIPT

protocols for protein immobilization is being endeavored.

In addition to transportation strategies, the controlled and monitored release of proteins from the nanocarriers is equally vital for avoiding unexpected extracellular burst release [14]. A possible approach for tracking protein release in an *in-situ* manner may draw a lesson from a photo-imaging strategy. Silica based nanomaterials functionalized with fluorescence compounds have been developed for biological imaging purposes [15-17]. Under the excitation of 980 nm NIR laser, Tm/Yb co-doped fluorides nanocrystals exhibit forceful upconverted luminescence, making them ideal for cell imaging applications [18]. However, for current UC photoluminescent silica materials which generally consist of luminescent core and silica shell, the synthesis methodologies usually involves cumbersome procedures, and the thin silica shell limits its effective storage of functional molecules [19].

In this work, fine photoluminescent CaF_2:Yb^{3+},Tm^{3+} nanocrystals were embedded mesoporous silica nanoparticles (CaF_2:Yb,Tm@MSNs), and the up-conversion nanoparticles (UCNPs) synthesized were modified with amino groups at the surface. Bovine serum albumin (BSA) was used as a macromolecular protein model. The protein loading capacity, release kinetics and corresponding photoluminescent phenomena of UCNPs were studied (Scheme 1). More importantly, the superior efficacy of intracellular protein transport by this new delivery platform was demonstrated.

2. Experimental section

2.1 Synthesis of luminescent silica nanospheres

In a typical procedure, 0.2 g cetyltrimethylammonium bromide (CTAB, ≥99%, Sigma–Aldrich Inc.), 25 mL deionized water, 5 mL ethanol, 50 μL of triethanolamine (TEA, Sinopharm Chemical Reagent) were mixed and stirred at 60 ^{o}C for 30 minutes. Subsequently, 2 mL tetraethylorthosilicate (TEOS, Sigma–Aldrich Inc., USA) was added into the solution under stirring for 2 h. When white participate appeared, the solution was cooled down to the ambient temperature, and the precipitate was

ACCEPTED MANUSCRIPT

collected by centrifugation. After being air-dried at 80 ^{o}C, the particles were further calcined at 550 ^{o}C for 5 h to obtain MSNs. To incorporate CaF_2:Tm,Yb nanocrystals within MSNs, a mixed ionic solution of Ca^{2+}, Tm^{3+} and Yb^{3+} was prepared by dissolving their corresponding acetates in deionized water, and then added with trifluoroacetic acid (TFA, 99%，Sigma–Aldrich Inc.) under stirring overnight at 40 ^{o}C. Subsequently, 400 mg of the as-synthesized MSNs was added into 20 mL of the as-prepared solution and immersed for 24 h under stirring at 40 ^{o}C. The particles were then collected by centrifuging and dried at 80 ^{o}C for 3 h and sintered at 600 ^{o}C for 3 h. The functionalization of luminescent nanoparticles with amino groups was then carried out following the modified existing protocols. Briefly, 100 mg of as-prepared particles was dispersed in 100 ml ethanol under sonication for 30 min, and 1.5 mL 3-aminopropyltriethoxysilane (APTES, Sinopharm Chemical ReagentCo., Ltd.) was added dropwise. After stirring for 24 h at 40 ^{o}C, the samples were collected by centrifugation and washed with ethanol to remove the excessive APTES molecules.

2.2 In vitro cytotoxicity assay

Cytotoxicity of luminescent nanosphere was assessed using fibroblast by Cell Counting Kit-8 method (CCK-8; Dojindo, Kamimashiki-gun Kumamoto, Japan). Briefly, cells were seeded into 96-well plate and incubated with particles for 24 hours and 48 hours. The particles concentration was ranged from 0 to-200 μg mL^{-1}. At each time point, the medium was refreshed, and 10 μL of CCK-8 solution was added and incubated at 37 ^{o}C for 4 hours. The cytotoxicity of nanospheres was examined by measuring the absorbance at 450 nm using a microplate reader (BIO-TEK Instruments, Minneapolis, USA).

2.3 Loading and release of BSA protein

Bovine serum albumin (BSA, 99%, Sigma–Aldrich) was dissolved in 20 mL phosphate buffer solution (PBS) at pH 7.4 to produce a stock solution with a concentration of 2 mg mL^{-1}. Unmodified and amino-modified nanoparticles (50 mg)

ACCEPTED MANUSCRIPT

were added into BSA solution at ambient temperature. The mixture was subsequently stirred for 24 h at room temperature to achieve the equilibrium state. The BSA-loaded nanoparticles were then collected by centrifugation and washed with PBS to remove the excess BSA protein. The *in vitro* BSA protein releasing test was performed by immersing the BSA loaded nanoparticles in 20 mL of PBS (pH=7.4) at 37 ± 0.1 ^{o}C. At predetermined time intervals, a 10 mL buffer solution was collected and immediately replaced with an equal volume of fresh PBS. The amount of BSA released in PBS solution was measured using a UV–vis spectrophotometer (TU-1810, China) at an absorbance of characteristic wavelength (λ=278–280 nm). Three measurements were performed for each sample.

2.4 Intracellular monitoring of BSA release.

Confocal microscopy luminescence imaging was carried out using a modified OLYMPUS FV1000 equipped a 980 nm laser diode. HepG2 cells (1×10^4/mL) were seeded onto a glass coverslips in 24-well plates and incubated for 24 h prior to cell culture. Subsequently, the original cell culture media was replaced with medium containing amino-modified UCNPs and BSA loaded amino-modified UCNPs (100 µg/mL). Subsequently, confocal microscopy luminescence imaging was carried out at scheduled time intervals. Upconversion luminescence of amino-modified UCNPs was detected under excitation at 980 nm laser.

2.5 In vitro cellular uptaking performance of BSA protein

HepG2 cells were seeded in 6- well plates in 2.0 ml of complete DMEM culture media (10 % FBS) at a density of 6×10^5 cells per well and incubated for 24 h under standard incubation conditions. Then, the original cell culture media were replaced with FITC-labeled BSA loaded nanoparticles (100 µg/mL) in 2.0 mL of complete DMEM culture media (10 % FBS) for each well and the cells were further incubated for 24 and 48 h. After removing the medium, the cells were washed with PBS for 3 times and fluorescence microscope (Nikon ECLIPSE Ti) was performed using to get

ACCEPTED MANUSCRIPT

the green fluorescence.

Flow cytometry analysis was performed to evaluate the BSA protein cellular uptake efficiency quantitatively. HepG2 cells were seeded in 6-well plates at a density of 6×10^5 cells per well and incubated for 24 h. Then, the original cell culture media was replaced with FITC-labeled BSA loaded nanoparticles (100 μg/mL) in 2.0 mL of complete DMEM culture media (10 % FBS) for each well. After cultured for 24 and 48 h, the media was removed. Then, the cells were trypsinized, washed with PBS, centrifuged, and resuspended in PBS buffer. Flow cytometry (NovoCyte 3130 (DEMO)) was carried out to measured the cell up-taking efficiency. Cells without FITC-labeled BSA loaded nanoparticles incubation were used as a control.

2.6 Characterization

The morphology of particles was characterized by field-emission scanning electron microscopy (FESEM, Hitachi SU-70, Japan) operated at 3 kV and high-resolution transmission electron microscopy (HRTEM, Tecnai F20, FEI, USA) operated at 200 kV. The phase and crystal structure were characterized by an X-ray diffraction instrument (XRD, X'Pert PRO MPD, The Netherlands) operating at 40 mA and 40 kV using Cu Kα radiation. The scan range was set at $20° < 2\theta < 60°$ with a step size of 0.167°. The FTIR spectra were recorded on a PerkinElmer 580B infrared spectrophotometer on KBr pellets (Tensor 27, Bruker, Germany) in the frequency range of 4000–400 cm^{-1} with a resolution of 4 cm^{-1}. Thermogravimetry/differential scanning calorimetry (TG-DSC, DSCQ1000, AT, USA) was used to measure the quantity of BSA loaded onto the nanoparticles in air with a heating rate of 10 ^{o}C/min from 25 to 700 ^{o}C. The upconversion photoluminescence spectra were recorded at room temperature under excitation by 980 nm laser from a fluorescence spectrophotometer (PL, FLSP920, Edinburgh). To minimize experimental accidental error, the sample positions and the spectra collection were maintained in identical conditions.

ACCEPTED MANUSCRIPT

3. Results and Discussion

3.1. Characteristics of CaF_2:Tm,Yb@$mSiO_2$ up-conversion nanoparticles (UCNPs)

The approach for synthesizing CaF_2:Tm,Yb@$mSiO_2$ UCNPs involved the preparation of mesoporous SiO_2 nanoparticles as templates, followed by the formation of CaF_2:Tm,Yb nanocrystals within its mesopores. TEM images of the as-prepared MSNs (Fig. S1) indicate the typical porous structure. Further, N_2 adsorption/desorption examination was performed to quantify the specific surface area and pore-size distribution. Apparent mesoporous characteristics of plateau regions were observed for the MSNs (Fig. S2). The specific surface area and pore volume of particles are ~729.3 m^2/g and ~0.725 cm^3/g, respectively. The average pore size of MSNs is ~5.04 nm (Table S1). The UCNPs synthesized exhibited uniform morphology and narrow size distribution with an average diameter of ～65 nm (Fig 1a). The examination using energy dispersive spectroscopy (EDS) confirmed the homogeneous distribution of Si, O, Ca, F, Yb and Tm elements within MSNs matrix (Fig S3). The microstructure of UCNPs was examined using TEM (Fig 1b-c). It was found that a large number of 'dark spots' (with dimensions up to 3~5nm) distribute homogeneously within the matrix of MSNs. In addition, the SAED pattern shows distinct diffraction rings, implying the crystalline nature of the spots formed. The lattice fringes of crystalline phase are clear in the HRTEM image, and the distance between the adjacent lattice fringes of nanocrystals imbeded is ~0.193 nm, which is well consistent with the interplanar spacing of (220) of cubic CaF_2 phase [20]. The XRD pattern of UCNPs confirms the presence of cubic CaF_2 phase (JCPDS No. 35-0816) due to the presence of well-defined diffraction peaks at (111), (220) and (311), as well as the amorphous silicon dioxide phase (Fig 1d) [21]. No additional impurities were observed. The findings suggest CaF_2 nanocrystals were successfully incorporated within MSNs matrix. When UCNPs were excited under 980 NIR laser, three narrow-band emission peaks at ～478 nm,～650 nm and ～800 nm presented

ACCEPTED MANUSCRIPT

(Fig 1e), and the particles showed a blue color. The emission spectra observed correspond to the electron transitions of Tm^{3+} ions: $^1G_4 \rightarrow {}^3H_6$ (~478 nm), $^3F_2 \rightarrow {}^3H_6$ (~650 nm) and $^3H_4 \rightarrow {}^3H_6$ (～800 nm) [22]. Further, with the increased particle concentration from 0 to 200 μg mL^{-1}, the relative cell viability with respect to the blank control retained over 90% viability after incubation for 24 and 48 h (Fig. 1f), reflecting low cell cytotoxicity of the particles synthesized.

3.2 In vitro protein loading and releasing behavior

The UCNPs prepared was subsequently surface-modified with amino groups to favor the protein loading procedure [23]. After surface modification, the appearance of the bonds at 2927 cm^{-1}, 2870 cm^{-1} and 1560 cm^{-1} confirms the successful attachment of amino groups in organosilane at the surface of UCNPs (Fig. 2a). In consequence, the zeta potential of UCNPs varied from -15.6 mV to 30.3 mV owing to positive surface modification with amino groups (Fig. 2b). The nitrogen adsorption-desorption isotherm and corresponding textural parameters of UCNPs and amino-modified UCNPs are provided in Fig. 3 and Table 1, respectively. After amino modification, the surface area was reduced from 563.3 m^2/g to 234.6 m^2/g, and pore volume is decreased from 0.68 cm^3/g to 0.42 cm^3/g accordingly, that agrees well with previous studied [24]. The weakened nitrogen adsorption is induced by the blockage of pores on UCNPs by amino groups attached. The CCK-8 assay using fibroblast confirmed that amino-modified UCNPs, with varied concentrations from 10 μg/mL up to 200 μg/mL, present at a high relative cell viability, reflecting its low cell cytotoxicity and good cytocompatibility (Fig. S4). In addition, amino-modified UCNPs with varied concentrations were dispersed in phosphate buffer saline (PBS) and simulate body fluid (SBF) solutions under irradiation using a laser point. Distinct 'Tyndall' phenomena confirm the excellent colloidal stability of amino-modified UCNPs (Fig. S5). Under 980 nm NIR laser excitation, the surface modification did not induced wavelength shift of photoluminescent emission peaks (Fig. S6), but the relatively intensity of blue emission at ~478 nm decreased owing to the presence of

ACCEPTED MANUSCRIPT

quenching groups in APTES molecules [25].

The FTIR spectra of UCNPs and amino-modified UCNPs after BSA loading are depicted in Fig. 4a. The infrared spectrum of BSA molecules consists of two amide peak regions, which are region I (2900–3000 cm^{-1}) and II (1500–1700 cm^{-1}). When particles were immersed in BSA solution for 24 h, absorption bands assigned to amide at ~1540 cm^{-1}, ~1650 cm^{-1} and CHx bond at ~2960 cm^{-1} were observed, confirming successful protein loading for both particles. TG curves in Fig. 4b show that, before BSA loading procedure, a marginal weight loss for UCNPs was induced due to the removal of adsorbed water, whereas the removed component for the amino-modified UCNPs system includes grafted APTES molecules as well as adsorbed water, resulting in increased weight loss. In contrast, after BSA protein loading, the weight loss of UCNPs (without surface modification) is ~5.3%, indicating its loading capacity. For amino-modified UCNPs, however, although the BET surface area and pore volume are reduced due to amino-functionalization, the BSA protein loading capacity is increased remarkably to ~10.5 %. In general, BSA is negative charged at pH 7.4, and the zeta potential of UCNPs varied from -15.6 mV to 30.3 mV after amino modification. Negative charged BSA protein molecules interact favorably with positive charged UCNPs after amino-modification *via* electrostatic bonding [26]. Furthermore, the amino groups at the surface may also interact with BSA molecules by a hydrophilic absorption. Both mechanisms induce its high loading capacity [27]. Therefore, the amino-functionalized UCNPs exhibit significantly enhanced protein loading capacity.

High loading capacity and sustained release behavior are expected but challenging aspects for intracellular protein delivery. UCNPs and amino-modified UCNPs after BSA protein loading were immersed in phosphate buffered saline (PBS, pH = 7.4) to enable the spontaneous protein release. As shown in Fig. 4c, both systems exhibit highly varied releasing phenomena. Within the initial 5 h, ~50 % of BSA contents is released from UCNPs, and in contrast only ~20% of total BSA molecules is liberated from amino-modified UCNPs. After 50 h, major BSA molecules

ACCEPTED MANUSCRIPT

have been released from unmodified UCNPs. In contrast, the total amount of BSA released is only ~35% for amino-modified UCNPs. UCNPs after amino-modification do not only present enhanced protein loading capacity but also induce significantly sustained release kinetics. For unmodified UCNPs, protein molecules, usually with large dimension, can hardly diffuse into the mesopores of MSNs and instead attach at the surface [26]. Meanwhile, UCNPs present a negative surface charge due to hydroxyl groups of MSNs matrix at the surface, and BSA molecule presents a negative net charge at pH 7.4. Thus, both UCNPs and BSA molecules were negatively charged in the neutral environment. The interaction between them belongs to physical adsorption [28, 29]. In this case, a 'burst' release phenomenon is more likely to occur [30]. However, for the amino-modified system, the more sustained releasing is induced by the ionic interaction between negative charged BSA molecules and the positive charged NH_2 groups at the surface of UCNPs, which enhances the stability of the immobilized protein and markedly reduces the amount of leaching. Therefore, the release process of BSA molecules from the nanocarriers was dramatically postponed. In addition, the decreased surface area and pore volume may also facilitate the enduring BSA releasing. Such enhanced protein storage and sustained releasing properties of nanocarrier are beneficial for reducing the repeated administration and the delivery efficiency of macromolecular proteins to the cell.

3.3 Optical-monitored BSA protein release process

Monitoring of protein releasing progress in a real time manner is one iconic feature for modern multifunctional delivery systems. Owing to the intrinsic up-conversion (UC) photoluminescent characteristics of UCNPs designed, the relationship between the UC emission intensity of both BSA loaded UCNPs and protein release progress was uncovered. As shown in Fig. 5 (a-c), accompanying with BSA releasing, the intensity of blue emission (~478 nm) increases with the cumulative releasing progress, while the red emission intensity remained barely changed. The reason might be that the BSA molecules can be adsorbed onto the

ACCEPTED MANUSCRIPT

surface of porous silica nanoparticles and quench some luminescent centers [31]. In general, the emission of rare earth ions is quenched by the environment with high phonon frequency [32]. The organic groups in BSA with high vibration frequencies from 1000 to 3500 cm^{-1} quench the emission of Tm^{3+} by a certain degree. It was also reported that the presence of organic ligands and OH groups may result in the quenching of green emission in $NaYF_4$ nanoparticles codoped with Yb^{3+} and Er^{3+} [33]. In this work, BSA molecules attached at the surface of UCNPs may selectively quench the blue emission. In consequence, for UCNPs samples, the blue emission recovers in a relatively rapid fashion due to its fast protein release kinetics, and meanwhile a delayed blue emission recoverage was observed when using amino-modified UCNPs for BSA delivery. The variation of photoluminescent phenomenon has thus been confirmed to effectively reflect the protein releasing progress.

The images of cells via the emission of amino-modified UCNPs were investigated using a modified confocal laser scanning microscopy (CLSM) equipped with infrared laser excitation at 980 nm. Hep G2 cells were incubated with amino-modified UCNPs (100 μg/mL) at 37 ^{o}C for 24 h prior to imaging procedure. As shown in Fig. 6, bright-field measurements after the treatment with amino-modified UCNPs confirm that the cells are viable throughout the imaging experiments. Moreover, an intense UC blue luminescence signal was observed from the Hep G2 cell under laser excitation at 980 nm. Overlays of bright-field and UC luminescent images demonstrate that the luminescence presents in the intracellular region. In contrast, the control group presents no UC luminescence signal under excitation using 980 nm laser. To shed light on protein release monitoring within living cells, Hep G2 cells were incubated with BSA protein loaded amino-modified UCNPs (100 μg/mL) at 37 ^{o}C for different period. A set of CLSM images were recorded to visualize the evolution of UC luminescence during intracellular protein release for 1, 3, 24, or 48 h. As shown in Fig. 7, a clear enhancement of blue emission signal was observed as increasing incubation time. Generally, cellular uptaking behavior of silica nanoparticles (NPs) is a time-dependent increase manner [34]. Previous studies have

ACCEPTED MANUSCRIPT

demonstrated that the cell-uptaking process of silica NPs occurs in the initial 10 h [34, 35]. The sustained release profile of amino-modified UCNPs in cell-free solution indicates that as low as ~19% of BSA released within 3 h, and only ~30% of total protein loaded released within 24 h (Figure 4c). The major content of protein remained within the nanoparticles prior to the up-taking process by cells, and thus the luminescent intensity of the amino-modified UCNPs remained quenched by the protein loaded. The PL-quenched UCNPs uptaken by cells can not present the blue emission with a high magnitude under 980 nm excitation. Therefore, the increased amount of UCNPs within cells may not induce such clear increase of blue light signal. The dramatic increase of blue light during cell culture is therefore mainly attributed to the releasing of the protein loaded. Therefore, the phenomenon observed reflects the effective monitoring of protein release within cells.

3.4 In vitro cellular up-taking of BSA protein

Efficient cellular up-taking plays a fundamental role in protein delivery applications [36]. The intracellular delivery efficiency of BSA protein was preliminarily evaluated using Hep G2 cancer cells. The cells were incubated with blank control, free FITC-BSA solution, FITC-BSA-loaded UCNPs, and FITC-BSA-loaded amino-modified UCNPs, respectively. As the fluorescence microscope images revealed in Fig. 8a, the cellular up-taking efficiency for cells cultured with free FITC-BSA solution presented at a low magnitude after 24 h incubation as the naked protein molecules can hardly penetrate into cells [4]. When cultured with FITC-BSA loaded UCNPs and amino-modified UCNPs systems, the cellular up-taking effect was significantly enhanced compared to the blank control. Amino-modified UCNPs system presented remarkably enhanced fluorescent activity induced by FITC-BSA cellular up-taking than unmodified UCNPs. The increase of fluorescence intensity within the cells indicates that the FITC-BSA protein was successfully delivered into cancer cells. After prolonged incubation for 48 h, the fluorescent activity for both UCNPs and amino-modified UCNPs systems were further enhanced, while the cells cultured with

ACCEPTED MANUSCRIPT

free FITC-BSA solution remained in dark due to the absence of any fluorescent activity within cells. The cells cultured with amino-modified UCNPs induced the strongest green fluorescence than other samples. The internalization of FITC-BSA molecules by the cells was analyzed quantitatively by flow cytometry (Fig. S7). As summarized in Fig. 8b, the protein up-taking efficiency by UCNPs and amino-modified UCNPs systems was determined to be ~27.9 % and ~49.4% after 24 h cell culture, respectively, and it reached ~56.8 % and ~73.6% after 48 h incubation. It is clear that amino-modified UCNPs system induced the remarkably enhanced cell up-taking efficiency owing to its high protein loading capacity. It is also noted that the prolonged incubation leads to increased cell up-taking efficiency for both systems. Such increasingly amplified protein up-taken efficiency induced by amino-modified UCNPs could be attributed to its high loading capacity and sustained intracellular release of protein molecules after particle internalization by cells.

4. Conclusions

Fine CaF_2:Tm,Yb nanocrystals were incorporated within the mesopores of silica nanospheres. After surface modification with amino groups, the protein loading capacity was remarkably increased from 5.3 % to 10.5 %. Meanwhile, the amino-modified UCNPs present a more sustained release profile of BSA protein due to the electrostatic bonding formed between BSA molecules and amino groups. Additionally, the upconversion emission intensity of the nanoparticles corresponded well with the protein releasing progress. The preliminary *in-vitro* study using Hep G2 cancer cells confirmed that amino-modified UCNPs induced significantly enhanced protein up-taking efficiency (up to ~73.6%) after 48 h. Owing to the excellent cellular uptaking performance and low toxicity, this new multifunctional protein delivery system may therefore offer a promising platform for intracellular delivery of various macromolecular proteins.

ACCEPTED MANUSCRIPT

Acknowledgements

This work was financially supported by National Nature Science Foundation of China (51232006, 51672247), Major State Research Program of China (2016YFC1101900) and Nature Science Foundation of Zhejiang Province (LY15E020005). Yangyang Li and Xiaoyi Chen contributed equally to this work

References

[1] S. R. Schwarze, A. Ho, A. V. Akbani, S. F. Dowdy, In vivo protein transduction: delivery of a biologically active protein into the mouse, Science 285 (1999) 1569-1572.

[2] M. Tyers, M. Mann, From genomics to proteomics, Nature 422 (2003) 193-197.

[3] B. Leader, Q. J. Baca, D. E. Golan, Protein therapeutics: a summary and pharmacological classification, Nat. Rev. Drug Discovery 7 (2008) 21-39.

[4] S. S. Bale, S. J. Kwon, D. A. Shah, A. Banerjee, J. S. Dordick, R. S. Kane, Nanoparticle-mediated cytoplasmic delivery of proteins to target cellular machinery, ACS nano 4 (2010) 1493-1500.

[5] W. Jiskoot, T. W. Randolph, D. B. Volkin, C. R. Middaugh, C. Schoneich, G. Winter, W. Friess, D. J. A. Crommelin, J. F. Carpenter, Protein instability and immunogenicity: roadblocks to clinical application of injectable protein delivery systems for sustained release, J. Pharm. Sci. 101 (2012) 946-954.

[6] K. Fu, A. M. Klibanov, R. Langer, Protein stability in controlled-release systems, Nat. Biotechnol. 18 (2000) 24-25.

[7] A. Sood, R. Panchagnula, Peroral route: an opportunity for protein and peptide drug delivery, Chem. Rev. 101 (2001) 3275-3303.

[8] Z. Gu, A. Biswas, M. X. Zhao, Y. Tang, Tailoring nanocarriers for intracellular protein delivery, Chem. Soc. Rev. 40 (2011) 3638-3655.

[9] S. Chen, X. T. Shi, A. Osaka, H. Gao, N. Hanagata, Facile synthesis, microstructure and BMP-2 delivery of novel silica hollow flowers for enhanced osteoblast differentiation, Chem. Eng. J. 246 (2014) 1–9.

[10] C. H. Lei, P. Liu, B. W. Chen, Y. M. Mao, H. Engelmann, Y. Shin, J. Jaffar, I. Hellstrom, J. Liu, K. E. Hellstrom, Local release of highly loaded antibodies from functionalized nanoporous support for cancer immunotherapy, J. Am. Chem. Soc. 132 (2010) 6906-6907.

ACCEPTED MANUSCRIPT

[11] I. I. Slowing, B. G. Trewyn, V. S.Y. Lin, Mesoporous silica nanoparticles for intracellular delivery of membrane-impermeable proteins, J. Am. Chem. Soc. 129 (2007) 8845-8849.

[12] C. Argyo, V. Weiss, C. Brauchle, T. Bein, Multifunctional mesoporous silica nanoparticles as a universal platform for drug delivery, Chem. Mater. 26 (2014) 435-451.

[13] M. Fujiwara, K. Shiokawa, I. Sakakura, Y. Nakahara, Silica hollow spheres with nano-macroholes like diatomaceous earth, Nano Lett 6 (2006) 2925-2928.

[14] S. Beyer, L. Xie, M. Schmidt, N. Bruin, M. Ashtikar, S. Ruschenbaum, C. M. Lange, V. Vogel, W. Mantele, M. J. Parnham, M.G. Wacker, Optimizing novel implant formulations for the prolonged release of biopharmaceuticals using in vitro and in vivo imaging techniques, J. Control Release 235 (2016) 352-364.

[15] C. X. Li , D. M. Yang , P. A Ma , Y. Y. Chen , Y. Wu , Z. Y. Hou ,Y. L Dai , J. H. Zhao , C. P. Sui , J. Lin, Multifunctional upconversion mesoporous silica nanostructures for dual modal imaging and in vivo drug delivery, Small 24 (2013) 4150-4159.

[16] X. B. Xu, S. Y. Lü, C. M. Gao, C. Feng, C. Wu, X. Bai, N. N. Gao, Z. Y. Wang, M. Z. Liu, Self-fluorescent and stimuli-responsive mesoporous silica nanoparticles using a double-role curcumin gatekeeper for drug delivery, Chem. Eng. J. 300 (2016) 185–192.

[17] Y. Y Chen, B. Liu, X. R. Deng, S. S. Huang, Z. Y. Hou, C. Xia Li, J. Lin, Multifunctional Nd^{3+}-sensitized upconversion nanomaterials for synchronous tumor diagnosis and treatment, Nanoscale 7 (2015) 8574-8583.

[18] Y. Y Li, Y. R. Zhou, X. Li, J. H. Sun, Z. H. Ren, W. J Wen, X. M Yang, G. R. Han, A facile approach to upconversion crystalline CaF_2:Yb^{3+},Tm^{3+}@$mSiO_2$ nanospheres for tumor therapy, RSC Adv. 6 (2016) 38365-38370.

[19] B. T. Chen, B. Dong, J. Wang, S. Zhang, L. Xu, W. Yu, H. W. Song, Amphiphilic silane modified $NaYF_4$:Yb,Er loaded with $Eu(TTA)_3(TPPO)_2$ nanoparticles and their multifunctions: dual mode temperature sensing and cell imaging, Nanoscale 5 (2013) 8541-8549.

[20] Y. Y. Li, Y. R. Zhou, T. X Gu, G. Wang, Z. H. Ren, W. J. Weng, X. Li, G. R. Han, C. B. Mao, A multifunctional nanocrystalline CaF_2:Tm,Yb@$mSiO_2$ system for dual-triggered and optically monitored doxorubicin delivery, Part. Part. Syst. Charact. 33 (2016) 896–905.

[21] Y. Y. Li, B. B. Li, G. Xu, Z. Ahmad, Z. H. Ren, Y. Dong, X. Li, W. J. Weng, G. R. Han, A feasible approach toward bioactive glass nanofibers with tunable protein release kinetics for bone scaffolds, Colloids Surf. B Biointerfaces 122 (2014) 785-791.

ACCEPTED MANUSCRIPT

[22] S. Sarkar, C. Hazra, V. Mahalingam, Bright luminescence from colloidal Ln^{3+}-doped $Ca_{0.72}Y_{0.28}F_{2.28}$ (Ln=Eu,Tm/Yb) nanocrystals via both high and low energy radiations, Chem. Eur. J. 18 (2012) 7050-7054.

[23] A. Martin, R. A. Garcia, D. S. Karaman, J. M. Rosenholm, Polyethyleneimine-functionalized large pore ordered silica materials for poorly water-soluble drug delivery, J. Mater. Sci. 49 (2014) 1437-1447.

[24] C. L. Tao, Y. F. Zhu, Y. Xu, M. Zhu, H. Moritac and N. Hanagatac, Mesoporous silica nanoparticles for enhancing the delivery efficiency of immunostimulatory DNA drugs, Dalton Trans. 43 (2014) 5142-5150.

[25] J. Pichaandi, F. C. J. M. V. Veggel, M. Raudsepp, Effective control of the ratio of red to green emission in upconverting LaF_3 nanoparticles codoped with Yb^{3+} and Ho^{3+} ions embedded in a silica matrix, ACS Appl. Mater. Inter. 2 (2010) 157-164.

[26] K. F. Wang, C. Chun Zhou, Y. L. Hong, X. D. Zhang, A review of protein adsorption on bioceramics, Interface Focus 2 (2012) 259-277.

[27] C. Lei, Y. Shin, J. Liu, E. J. Ackerman, Entrapping enzyme in a functionalized nanoporous support. J. Am. Chem. Soc. 124 (2002) 11242-11243.

[28] D. Baowan, V. Helms, Quantitative study of BSA coating silica nanoparticle, J Math Chem 53 (2015) 29-40.

[29] S. Hudson, J. Cooney, E. Magner, Proteins in mesoporous silicates, Angew. Chem. Int. Ed. 47 (2008) 8582-8594.

[30] S. Wang, M. Chen, L. Wu, One-step synthesis of cagelike hollow silica spheres with large through-holes for macromolecule delivery, ACS Appl. Mater. Interfaces 8 (2016) 33316–33325.

[31] Z. Y. Hou, X. J. Li, C. X. Li, Y. L. Dai, P. A. Ma, X. Zhang, X. J. Kang, Z. Y. Cheng, J. Lin, Electrospun upconversion composite fibers as dual drugs delivery system with individual release properties, Langmuir 29 (2013) 9473-9482.

[32] Z. Y. Hou, C. X. Li, P. A. Ma, G. G. Li, Z. Y. Cheng, C. Peng, D. M. Yang, P. P. Yang, J. Lin, Electrospinning preparation and drug-delivery properties of an up-conversion luminescent porous $NaYF_4$:Yb^{3+}, Er^{3+}@silica fiber nanocomposite, Adv. Funct. Mater. 21 (2011) 2356–2365.

[33] J. W. Zhao, Y. J. Sun, X. G. Kong, L. J. Tian, Y. Wang, L. P. Tu, J. L. Zhao, H. Zhang, Controlled synthesis, formation mechanism, and great enhancement of red upconversion luminescence of $NaYF_4$:Yb^{3+}, Er^{3+} nanocrystals/submicroplates at low doping level, J. Phys. Chem. B. 112 (2008) 15666–15672.

[34] J. Blechinger, A. T. Bauer, A. A. Torrano, C. Gorzelanny, C. Bräuchle, S. W. Schneider, Uptake kinetics and nanotoxicity of silica nanoparticles are cell type dependent, Small 9 (2013) 3970–3980.

ACCEPTED MANUSCRIPT

[35] Y. N. Yang, Y. T. Niu, J. Zhang , A. K. Meka, H. W. Zhang, C. Xu, C. X. C. Lin , M. H. Yu, C. Z. Yu, Biphasic synthesis of large-pore and well-dispersed benzene bridged mesoporous organosilica nanoparticles for intracellular protein delivery, Small 11 (2015) 2743–2749.

[36] Y. Y. Jiang, H. X. Lu, F. Chen, M. Callari, M. Pourgholami, D. L. Morris, M. H. Stenzel, PEGylated albumin-based polyion complex micelles for protein delivery, *Biomacromolecules* 17 (2016) 808-817.

Figure captions

Table 1. Texture properties of UCNPs before and after amino-modification.

Scheme 1. Schematic illustration of CaF_2:Tm,Yb@mSiO_2 nanospheres designed for protein delivery.

Figure 1. (a) SEM image (the inset shows nanosphere size distribution), (b) TEM images (the inset shows the corresponding SAED patterns), (c) HRTEM images, and (d) X-Ray diffraction patterns of crystalline CaF_2:Tm,Yb@SiO_2 nanospheres; (e) Photoluminescece spectrum under excited by 980 nm laser; (f) Relative cell viability of fibroblast incubated nanospheres with different concentrations for 24 h and 48 h.

Figure 2. (a) FTIR spectra, and (b) Zeta potential of the UCNPs before and after amino- modification.

Figure 3. (a) N_2 adsorption/desorption isotherm; (b) mesopore pore size distribution of UCNPs and amino-modified UCNPs.

Figure 4. (a) FTIR spectra of BSA molecules, BSA loaded UCNPs, BSA loaded amino-modified UCNPs (b) TG curves of UCNPs and amino-modified UCNPs before and after BSA protein loading, (c) Cumulative BSA protein release profiles of BSA-loaded UCNPs and amino-modified UCNPs in PBS (pH=7.4).

Figure 5. (a, b) Spectra of upconversion emission as a function of release time for BSA loaded UCNPs and amino-modified UCNPs , (c) Upconversion emission of the intensity ratio of blue ($^1G_4 \rightarrow {}^3H_6$ (~478 nm)) and red ($^3F_2 \rightarrow {}^3H_6$ (~650 nm)) (I_{blue}/I_{red}) as a function of release time.

Figure 6 Confocal laser scanning microscopy (CLSM) images of Hep G2 cell incubated

ACCEPTED MANUSCRIPT

with or without amino-modified UCNPs for 24 h under 980 nm excitation. The scale bar: 25 µm.

Figure 7. Confocal laser scanning microscopy (CLSM) images of Hep G2 cell incubated with BSA loaded amino-modified UCNPs as a function of release time under 980 nm excitation. The scale bar: 25 µm.

Figure 8. (a) Fluorescence microscopy images of Hep G2 cell cultured with FITC labelled BSA loaded amino-modified UCNPs and FITC labelled BSA loaded UCNPs, FITC labelled BSA and control. The scale bar is 100 µm, (b) Evaluation of cellular uptake of FITC labelled BSA protein by flow cytometry.

ACCEPTED MANUSCRIPT

ACCEPTED MANUSCRIPT

Table 1.

Samples	Surface Area (m^2/g)	Volume (cm^3/g)
UCNPs	563.3	0.68
Amino modified UCNPs	234.6	0.42

Scheme 1

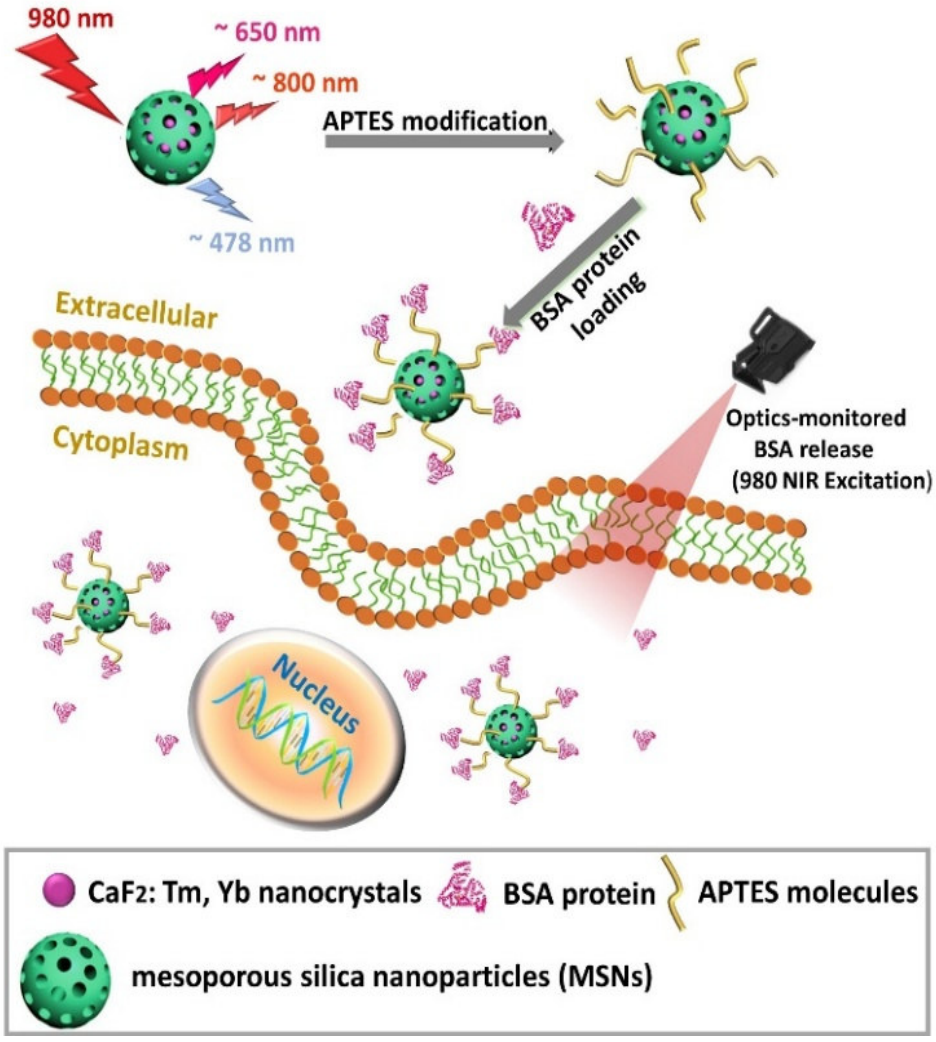

ACCEPTED MANUSCRIPT

Fig. 1

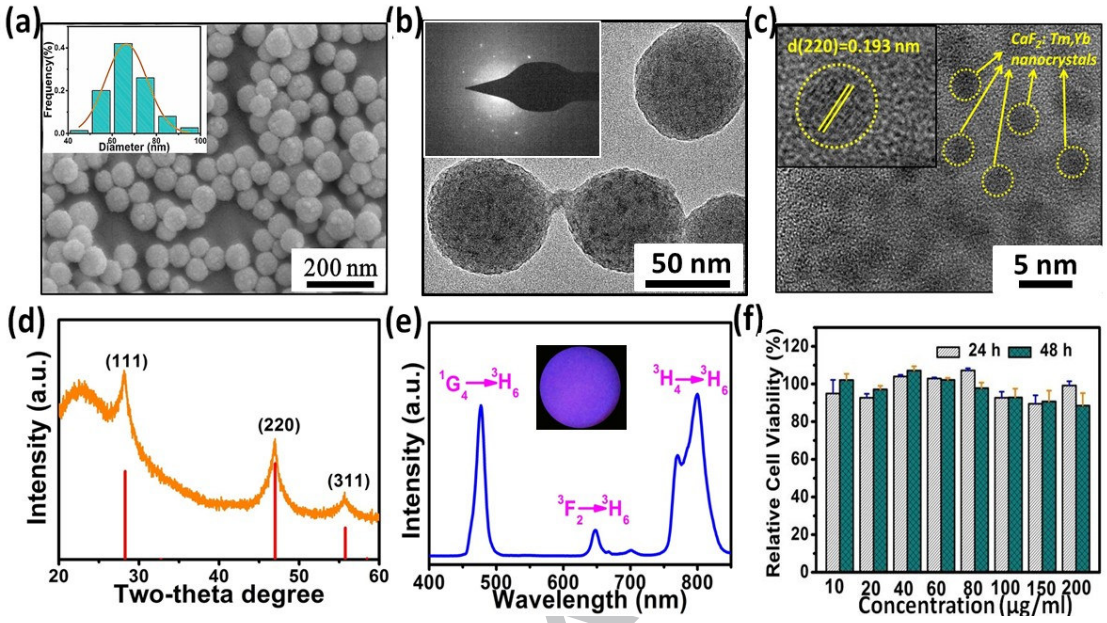

ACCEPTED MANUSCRIPT

ACCEPTED MANUSCRIPT

Fig. 2

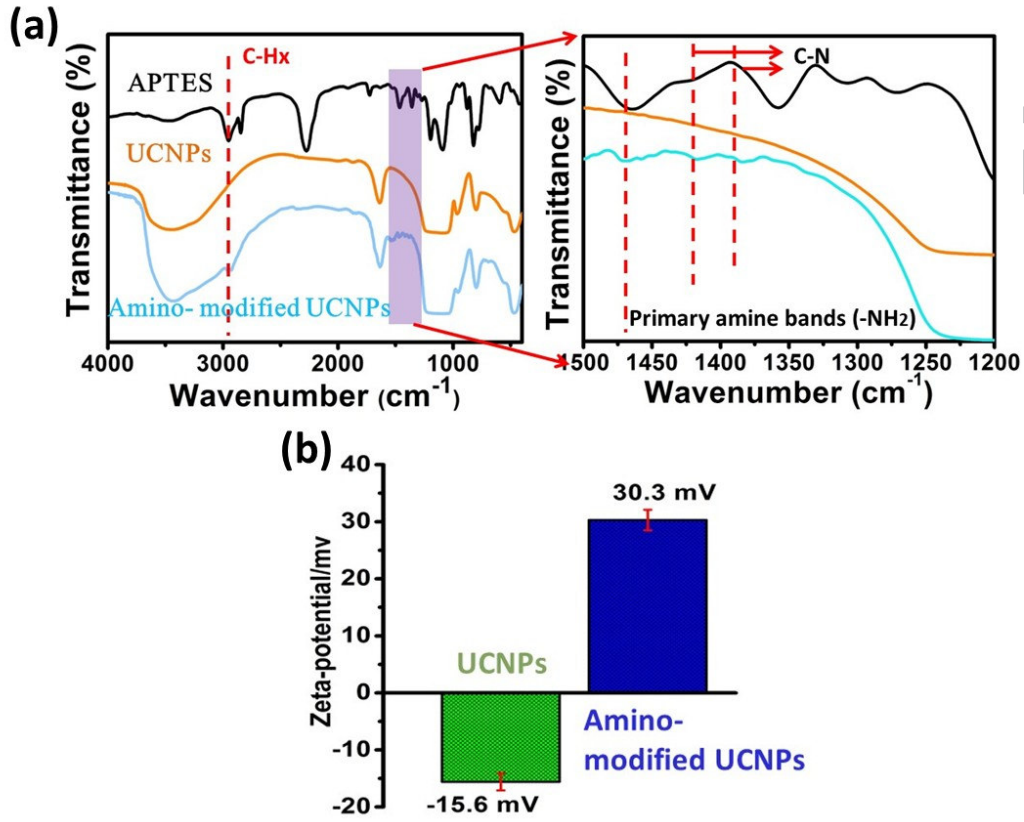

Fig. 3

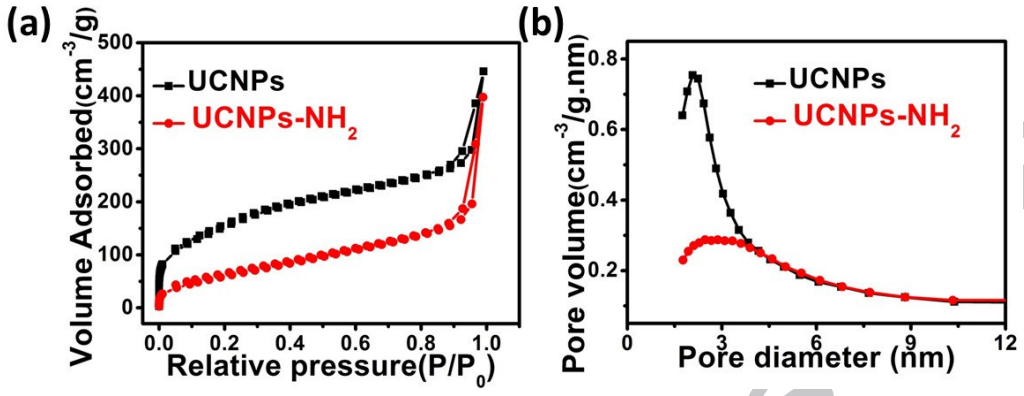

Fig. 4

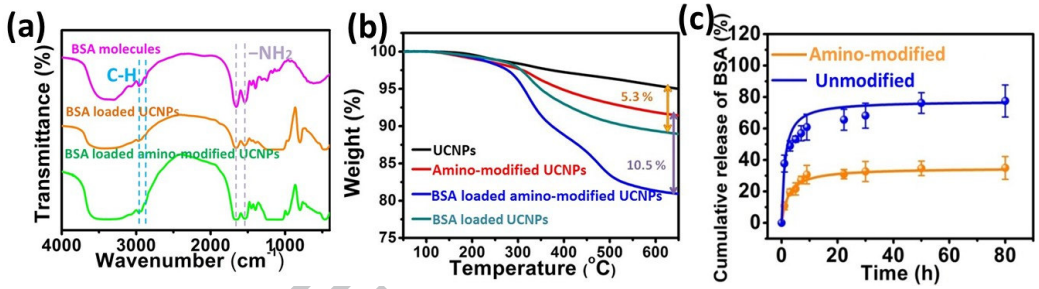

Fig.5

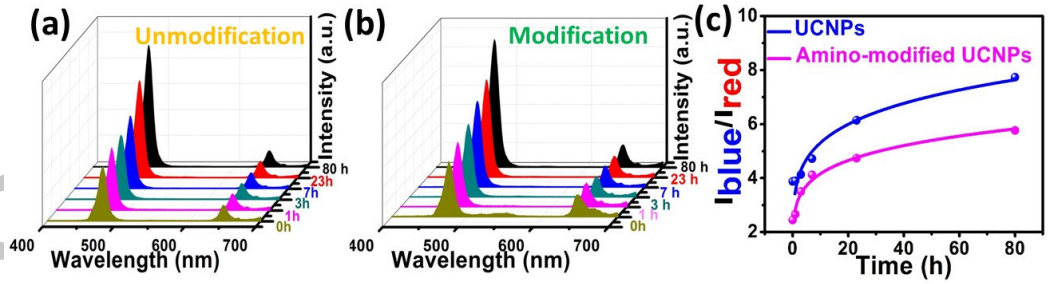

Fig. 6

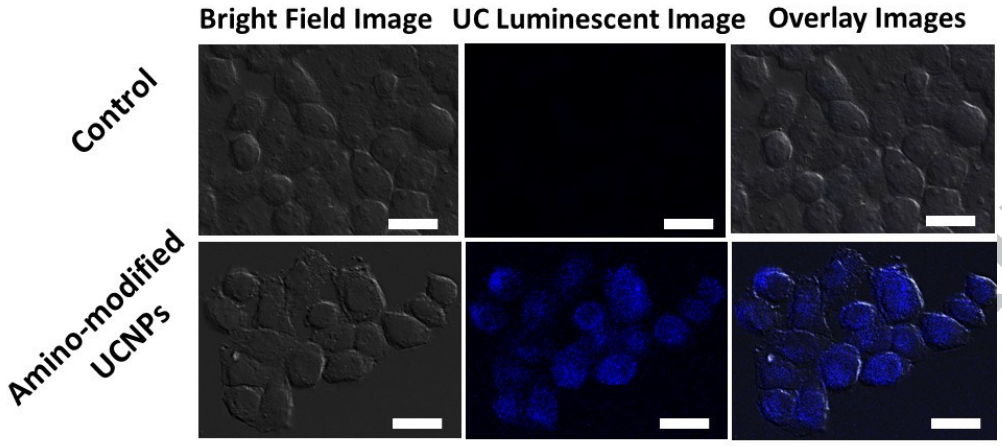
Bright Field Image
UC Luminescent Image
Overlay Images
Control
Amino-modified UCNPs

Fig.7

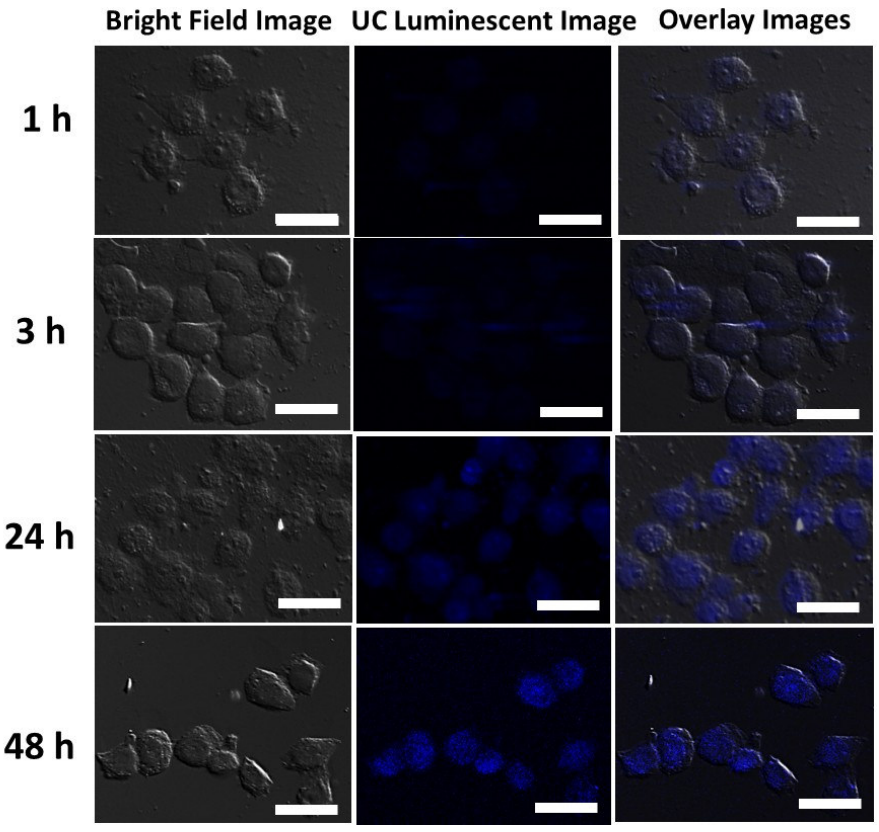
Bright Field Image
UC Luminescent Image
Overlay Images
1 h
3 h
24 h
48 h

ACCEPTED MANUSCRIPT

Fig. 8

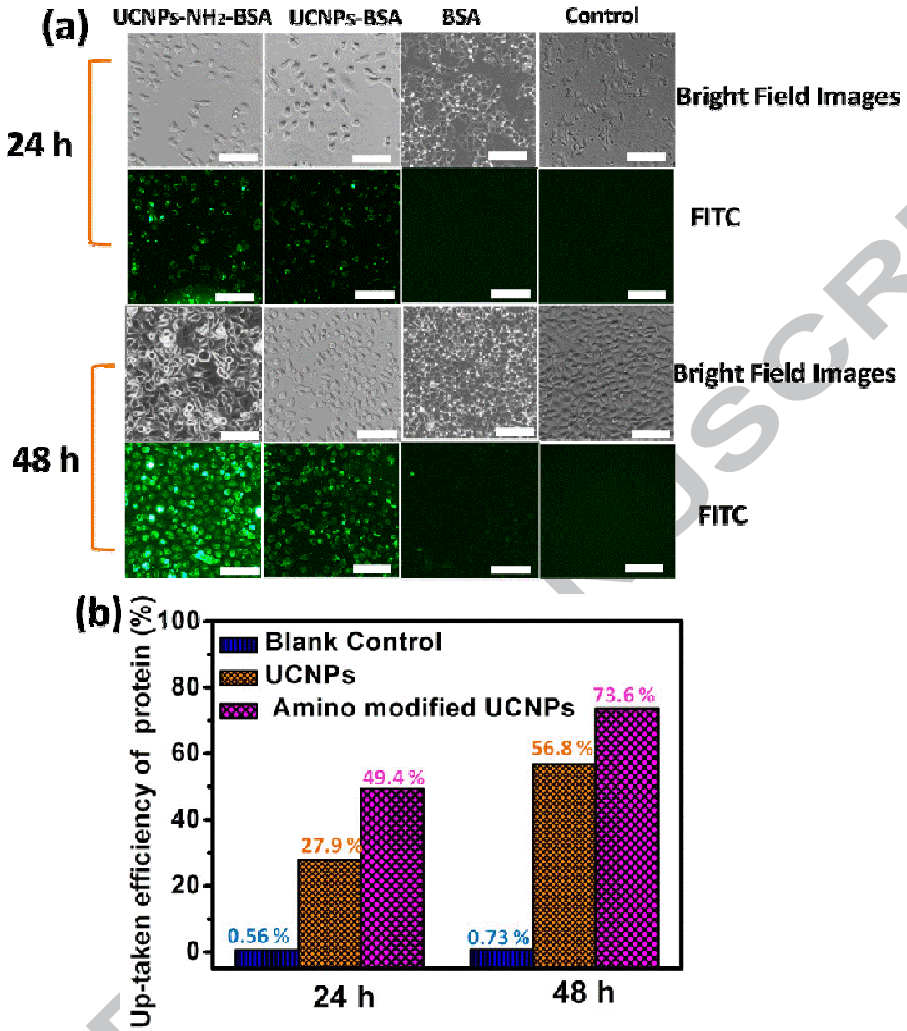

ACCEPTED MANUSCRIPT

Graphical Abstract

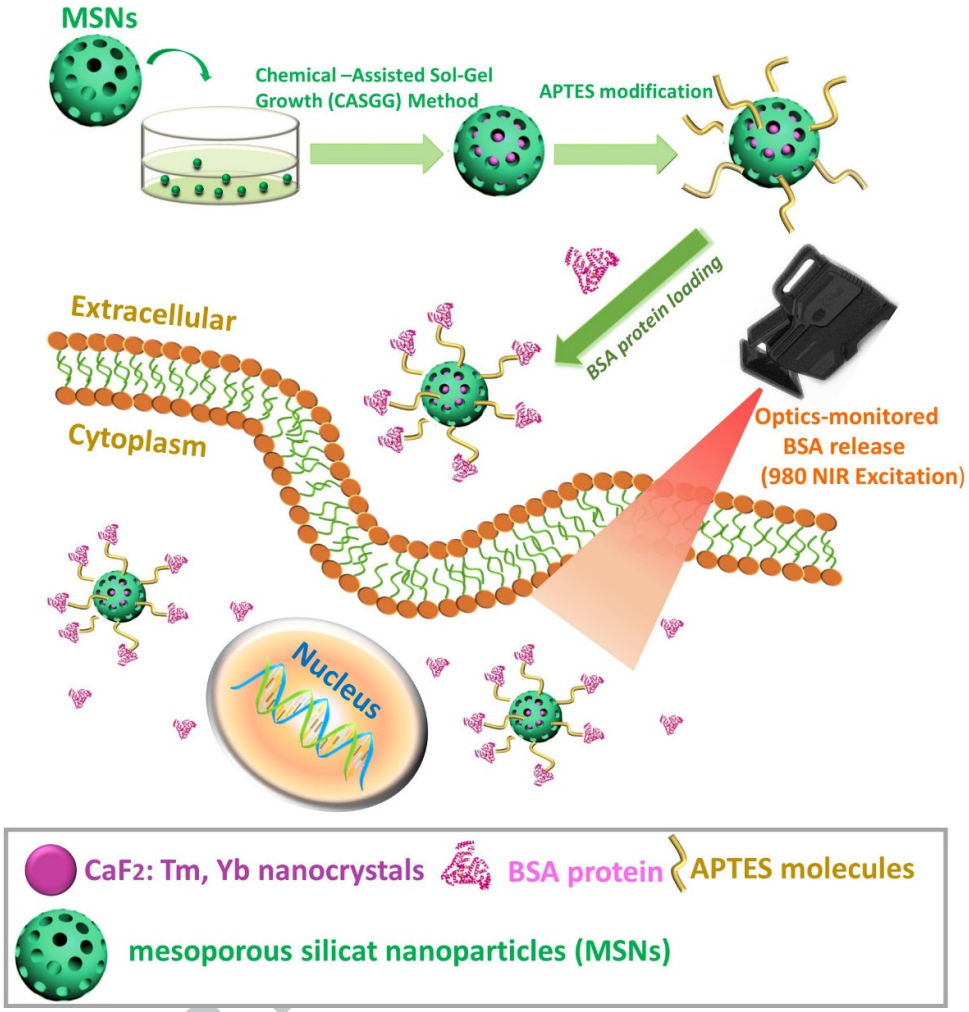

ACCEPTED MANUSCRIPT

Highlights

- *In situ* growth of photoluminescent nanocrystals within mesopores of MSNs;
- High protein loading and sustained release due to amino surface modification;
- Cell up-taking rate of protein reaches ~75%;
- Monitoring of protein release by the evolution of photoluminescence.

ACCEPTED MANUSCRIPT